

Wavelet based inversion of gravity data

Fabio Boschetti

CSIRO Exploration & Mining
and Australian Geodynamics Cooperative Research Centre
P.O. Box 437, Nedlands
Western Australia, Australia 6009
Telephone: (08) 9389 8421
Facsimile: (08) 9389 1906
E-mail: f.boschetti@ned.dem.csiro.au

Peter Hornby

CSIRO Exploration & Mining
and Australian Geodynamics Cooperative Research Centre
P.O. Box 437, Nedlands
Western Australia, Australia 6009
Telephone: (08) 9389 8421
Facsimile: (08) 9389 1906
E-mail: p.hornby@ned.dem.csiro.au

Franklin G. Horowitz

CSIRO Exploration & Mining
and Australian Geodynamics Cooperative Research Centre
P.O. Box 437, Nedlands
Western Australia, Australia 6009
Telephone: (08) 9389 8421
Facsimile: (08) 9389 1906
E-mail: f.horowitz@ned.dem.csiro.au

Left Running Heading: Boschetti, Hornby, and Horowitz

Right Running Heading: Wavelet based inversion of gravity data

ABSTRACT

The Green's function of the Poisson equation, and its spatial derivatives, lead to a family of wavelets specifically tailored to potential fields. Upward continuation of the field is seen to be identical to these wavelets' scale change operation. The maxima at all heights of the field's horizontal gradients are termed the field's multiscale edges. A multiscale edge's field strength variation and geometry contain information about the geometry and type of discontinuity in the source. The assumptions that "rocks have edges" and that these discontinuities are represented in the field's multiscale edges appears to collapse much of the ambiguity inherent in the inversion of potential field data. One approach to inversion is purely visual, relying upon the way that multiscale edges for dipping fault blocks sometimes "mirror" the fault geometry. A second approach recovers the density contrast, the depths to top and bottom, and the dip angle of an isolated synthetic dipping fault block by performing a search for parameters that best recreate the observed multiscale edges. A third approach relies upon naïve downward continuation. When a field is downward continued below its actual source, a common assumption about the downward continuation operator is violated, introducing well known oscillatory components to the previously smooth result. Such oscillatory components tend to arise first on multiscale edges. By following multiscale edges as we downward continue, we can pick the maximum depth to a source (provided our "rocks have edges" assumption is true). Finally, since the gravity field wavelet is (proportional to) a Green's function for mass dipoles, we can directly interpret the wavelet transform itself as being (proportional to) a distribution of sources composed entirely of horizontal mass dipoles. Thus, multiscale edges can be interpreted as the modes of the probability density of edges in the source distribution generated by the wavelet transform.

Key Words: potential field inversions, wavelets, multiscale edges, source discontinuity structure.

1 INTRODUCTION

The accurate inversion of potential field data for their underlying sources is widely known to be both difficult and ambiguous. In two previous papers (Boschetti et al., 1999a; Hornby et al., 1999) we demonstrated respectively the range of ambiguity and a wavelet based analysis of potential fields. In this paper, we combine the previous two approaches and present a wavelet-based inversion of gravity data.

The aim of this inversion, like that of any geophysical inversion, is to decipher as much information about the underlying rocks as possible from the limited set of information available. We would be satisfied to be able to delineate the geometry and position of anomalous bodies, but would ideally like to be able to infer more information (such as physical properties, or even chemical composition). In practice, the former goal proves difficult enough, while the latter goal seems unattainably difficult.

1.1 Ambiguity

An independent analysis of ambiguity, resulting in the same nullspace formulation as the one in Boschetti et al. (1999a), may be found in Strykowski (1996).

The fundamental mathematical difficulty with voxel based inversion of potential fields arises because there are never enough measurements to constrain all of the available degrees of freedom in the inversion. While we describe the arguments supporting this point of view at great length in Boschetti et al. (1999a), the quick way to see this is via the following argument. Suppose a gravity survey is gridded to some chosen resolution, and it is desired to invert for the underground structure at the same (horizontal) resolution. Obviously, the number of constraint equations is finite (call it N , the number of cells in the gridded measurement field). Equally obvious is the fact that a single layer of underground source unknowns would exhaust the N constraints, even if the inversion were only for density (as opposed to density and some other physical property, such as acoustic velocity, correlated to the measurements). More layers would require more constraints, which have to come from somewhere.

Nevertheless algorithms for multi-layered voxel inversion abound in the literature. How could they possibly work? The answer must lie in the prior information the algorithms bring to bear upon solving the inversion problem. Clearly by the “equivalent” layer argument in the previous paragraph, for multi-layered source inversions the *a priori* information constrains more degrees of freedom than does the information from the potential field measurement itself. Hence the nature and quality of the prior information is crucial to the success of inversion.

Because the constraints provided by the potential field measurement are so weak, relatively speaking, we also must be careful not to over-constrain the problem simply from the prior information (Boschetti et al., 1999a). A delicate balance is needed between mathematical parsimony on the one hand and geological common sense on the other.

We suggest that one such balance may be found in the statement “rocks have edges”. Or, more precisely, the balance is found in its generalisation to “rocks have piecewise constant densities/susceptibilities, punctuated by singularities”---which come in varieties more plentiful than edges.

If we require our inversions to honour this statement, two very useful properties emerge. Firstly, such an *a priori* constraint is of widespread geological applicability, and is easily verified for many regions under study. Secondly, wavelet based singularity detection and classification techniques can be used on the field itself, which (as we shall see shortly) allows for inversions at the full horizontal resolution of the gridded data, at an effectively continuous range of depths.

We emphasise that “rocks have edges” is an **assumed** constraint on the inversion described here. Inevitably, there will occur regions where such an assumption is not justified, and any source inversion obtained from this method will be wrong purely because this assumption has been violated.

Many families of wavelets exist, and many different kinds have been derived with specific properties (e.g. Daubechies, 1992; Kaiser 1994), or employed for various kinds of signal analysis (e.g. Mallat and Zhong, 1992; Sweldens, 1994; Strang and Nguyen, 1996).

One could perform a multiscale wavelet analysis on gravity data using any suitable choice of wavelets (e.g. the Haar system, or its generalisation, the Daubechies family of wavelets). Instead, we choose to derive a wavelet specifically for potential fields from the physics of the situation. This allows us to “marry” potential field theory with wavelet analysis, creating a natural synergy for analysing potential fields.

Our choice of wavelets has many benefits that, in our opinion, offset the difficulties we encounter in using these non-orthogonal, continuous, non-product wavelets. For example, the inverse wavelet transform has a direct physical interpretation in terms of a “gravitational dipole source distribution”. This leads naturally to the understanding that the wavelet transform we construct from our wavelets can be understood as a probability amplitude for horizontal edges. (There are two dipole polarisations in the x and y directions, forming two amplitudes, the sum of squares then forming the probability density for edges). One can then interpret the multiscale edges as the local modes of the associated edge probability density. This in turn leads us into the realm of Fisher information principles (e.g. Frieden, 1999), and the associated theory of inference in the presence of inherent unknowability in measurement processes. A vital connection here is that the wavelets are harmonic functions, which can be supposed as arising from a variational principle related to a Fisher information principal. Hence, the nature of the prior hypothesis underlying the particular edge density distribution constructed by the wavelet transform can be deduced. Nothing like this depth of understanding could arise as clearly from the use of any other wavelet.

The foregoing also opens an entire field of investigation regarding the handling of ambiguity in geophysical inversion systems. Whenever the wavelet transform can be interpreted as some sort of distribution of objects or features that generate the field in some way, then the particular wavelet basis we use, can be thought to induce an information principle, which in turn leads to identification of the hypotheses.

2 MULTISCALE ANALYSIS OF POTENTIAL FIELD DATA

In this section, we review the theory of wavelets derived explicitly for potential fields. The full development may be found in Hornby et al. (1999), and an alternative development in Moreau et al. (1997).

2.1 Definitions

Wavelet analysis pairs two related functions to analyse a signal. The first function called the smoothing function $\theta(x)$, when convolved with the signal under study, can be viewed as an operation that smoothes the signal to contain lengths dominantly longer than some characteristic length (which is a property of the function θ). In one dimension, to be admissible for wavelet analysis, θ must be non-negative, differentiable, and obey

$$\int_{\mathfrak{R}} \theta(x) dx = 1. \quad (2.1)$$

The second function – called the first order or “mother” wavelet function $\psi(x)$ – is taken as the first derivative of the smoothing function. Convolution with this function can be viewed as an operation that roughens the signal under study. In one dimension,

$$\psi(x) = \theta_{,1}(x) = D_x \theta(x). \quad (2.2)$$

(Note that D_x denotes differentiation with respect to x , and that, in preparation for more than one dimension, we have already introduced the comma sub-script convention to denote differentiation in the classical tensorial style). From these “mother” functions, wavelets are used to analyse a signal at multiple scales via the following constructions. The scaled version of θ is given by

$$\theta_s(x) = (1/s)\theta(x/s), \quad s > 0, \quad (2.3)$$

where s is the rescaling factor. Similarly, the scaled version of ψ is given by

$$\psi_s(x) = (1/s)\psi(x/s). \quad (2.4)$$

The wavelet transform of a signal $f(x)$ is then defined by

$$W[f](s, x) = [f * \psi_s](x), \quad (2.5)$$

where $(*)$ denotes convolution. Then we see that

$$W[f](s, x) = [f * (sD_x \theta_s)](x) = sD_x [f * \theta_s](x). \quad (2.6)$$

This shows that the wavelet transform $W[f](s, x)$ is, except for a scale factor s , the first derivative of the signal smoothed at the scale s . The local extrema (with respect to x) of $W[f](s, x)$ thus correspond to rapid variations in $[f * \theta_s]$, and hence can be interpreted as regions of rapidly changing intensity, i.e., edges in the signal $[f * \theta_s]$. Now, $[f * \theta_s]$ is just the original signal f blurred or averaged at scale s by the filter kernel θ_s . Consequently, the local maxima of $|W[f]|$ correspond to edges in the signal after blurring at scale s . These edges, which become a function of scale s , are termed **multiscale edges**.

2.2 Potential Field Wavelets

Following the development in Hornby et al. (1999), we start by considering the gravitational potential on a horizontal plane due to a density distribution ρ ,

$$V(x, y, z_0) = -G \int_{\mathbb{R}^2} dx' dy' \int_{-\infty}^0 \frac{\rho(x', y', z') dz'}{((x - x')^2 + (y - y')^2 + (z_0 - z')^2)^{1/2}}, \quad (2.7)$$

where V is the potential, x, y are the horizontal coordinates, $z=z_0$ is the (positive) height of the plane, G is the Newtonian gravitational constant, and the density distribution ρ is assumed zero for $z > 0$. (Positive z is “up”). From this we find that the *magnitude* of vertical acceleration f_{z_0} is

$$f_{z_0}(x, y) = -g_z = V_{,3} = G \int_{\mathbb{R}^2} dx' dy' \int_{-\infty}^0 \frac{\rho(x', y', z')(z_0 - z') dz'}{((x - x')^2 + (y - y')^2 + (z_0 - z')^2)^{3/2}}. \quad (2.8)$$

The Green’s function for the magnitude of vertical acceleration is

$$K(x, y, z) = \frac{z}{(x^2 + y^2 + z^2)^{3/2}}. \quad (2.9)$$

By direct calculation,

$$\int_{\mathbb{R}^2} K(x, y, z) dx dy = 2\pi \quad (2.10)$$

for any $z > 0$. Hence the integral of the function

$$\gamma_z(x, y) = \frac{1}{2\pi} K(x, y, z) \quad (2.11)$$

is unity for all $z > 0$.

From Equation (2.1) and the facts that γ_z is non-negative for $z > 0$ and differentiable, we see that γ_z is admissible as a smoothing function for a wavelet, with a corresponding scaled version

$$\begin{aligned} \gamma_{sz}(x, y) &= \frac{1}{2\pi} \frac{sz}{(x^2 + y^2 + (sz)^2)^{3/2}} . \\ &= s^{-2} \gamma_z(x/s, y/s) \end{aligned} \quad (2.12)$$

Equation (2.12) is the 2 dimensional analogue of Equation (2.3). We therefore define the scale $s=1$ by defining θ to be the normalised Green's function associated with height z_0 , that is

$$\theta(x, y) = \gamma_{z_0}(x, y) \quad (2.13)$$

and

$$\theta_s(x, y) = \gamma_{sz_0}(x, y) = s^{-2} \theta(x/s, y/s) . \quad (2.14)$$

As an aside, such a definition of scale appears problematic for gravity surveys measured at ground level ($z_0 = 0$). We proceed pragmatically. When such a situation arises, we choose some nominal z_0 (usually the interpolated grid or pixel spacing in the horizontal directions) and use this length to define $s=1$.

In the two dimensional case, the first order wavelet is a vector-valued function, with components given by

$$\psi^1 = \theta_{,1} = D_x \theta \quad \text{and} \quad \psi^2 = \theta_{,2} = D_y \theta . \quad (2.15)$$

The components

$$\psi_s^i(x, y) = s^{-2} \psi^i(x/s, y/s) \quad (2.16)$$

form a set of self consistent dilation equations for this 1st order wavelet.

The x component of the 2-D wavelet transform of $f_0(x, y)$ (the acceleration at zero height) is given by

$$\begin{aligned}
W^1[f_0](s, x, y) &= [f_0 * \psi_s^1](x, y) \\
&= f_0 * sD_x \theta_s \\
&= sD_x [f_0 * \theta_s] \\
&= sD_x [f_0 * \gamma_{sz_0}] \\
&= (z / z_0) D_x f_z(x, y)
\end{aligned} \tag{2.17}$$

where $s = z / z_0$. A similar result follows for the y component, and hence the full vector wavelet transform of the acceleration at zero height is

$$\vec{W}[f_0](s, \vec{x}) = (z / z_0) \vec{\nabla} f_z(\vec{x}), \tag{2.18}$$

where $\vec{\nabla}$ denotes the 2-D gradient operator in the x,y plane, and \vec{W} denotes a 2-D vector. In summary, we see that this particular wavelet transform of the acceleration at zero height can be calculated at scales $s > 1$ from measurements at height $z = z_0$ as follows,

1. upward continue the measured field to a level $z = sz_0$,
2. take the 2-D gradient in the (x,y) plane, and
3. multiply the resulting vector by the factor s.

Thus, no new processing software is needed to calculate these wavelet transforms. The tools and techniques are present in existing systems.

By analogy with Equation (2.6), we define multiscale edges to be located where \vec{W} takes on local maxima along each gradient streamline. Once again, this procedure finds the multiscale edges corresponding to rapid variations in $[f * \theta_s]$.

3 MULTISCALE EDGE BASED INVERSION

We now turn to inverting potential fields based on the information contained in their multiscale edges. Recall, from the first section, that we propose inverting based upon the assumption that “rocks have edges”. Hornby et al. (1999) derive the geometry

and amplitude scaling relations for the multiscale edges produced by various types of isolated source singularities. Using these relationships, we simply *assume* that any multiscale edge found in the potential field is associated with the best fitting type of singularity in the rock. This assumption is analogous to a common strategy employed by potential field interpreters, where they correlate “visual boundaries” in the field measurement with the boundaries of geological units. Indeed, emulation of this interpretation procedure was part of the motivation that led us to these investigations.

Note that the assumed correlation between edge and singularity could be violated in any number of ways. For example, isostasy can naturally lead to compensation that tends to damp anomalies. Such compensated singularities may well remain undetected. On the other hand, continuous variations of density will sometimes masquerade as singularities. Any spherical density anomaly will look like a point source.

3.1 Visual “Inversion”

The multiscale edges due to a horizontal layer truncated by a dipping fault plane can be partially “inverted” through a purely visual procedure (i.e. no computation is required). Section 3.2.1 of Hornby et al. (1999) describes the theory for the scaling of amplitude with height, and Figure 1 through Figure 3 display results for some numerical synthetics.

Note that the visual result is that the multiscale edges move (with upward continuation) in the direction of downward dip of the fault. Note also that the vertical asymptote of the multiscale edge moves farther from the surface intercept with decreasing dip angle. Crudely speaking, this class of multiscale edge behaves as if the ground surface is a (distorting) mirror. An interpreter can infer both the sense and magnitude of dip simply from a visual appraisal of the multiscale edge.

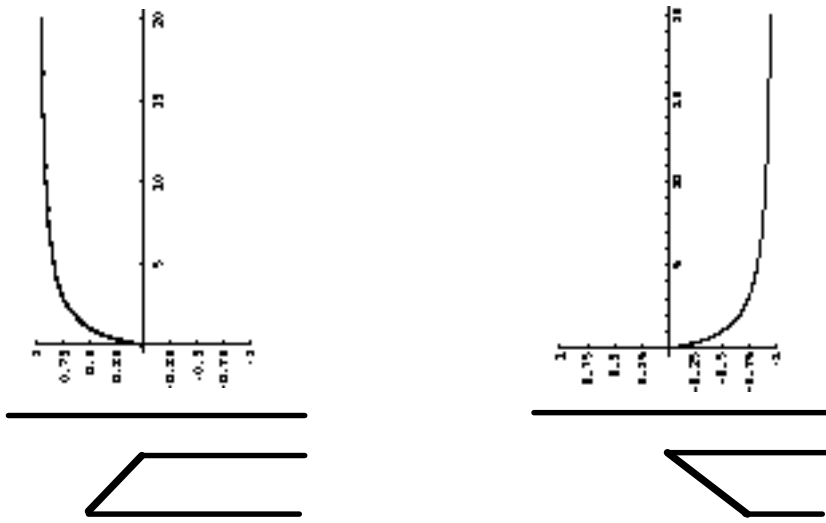


Figure 1. Faults dipping 45 degrees and multiscale edges at different heights.

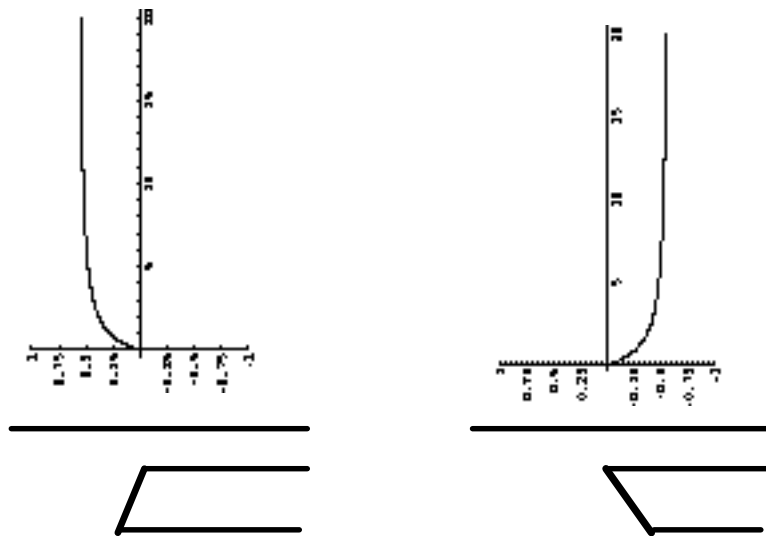


Figure 2. Faults dipping 60 degrees and multiscale edges at different heights.

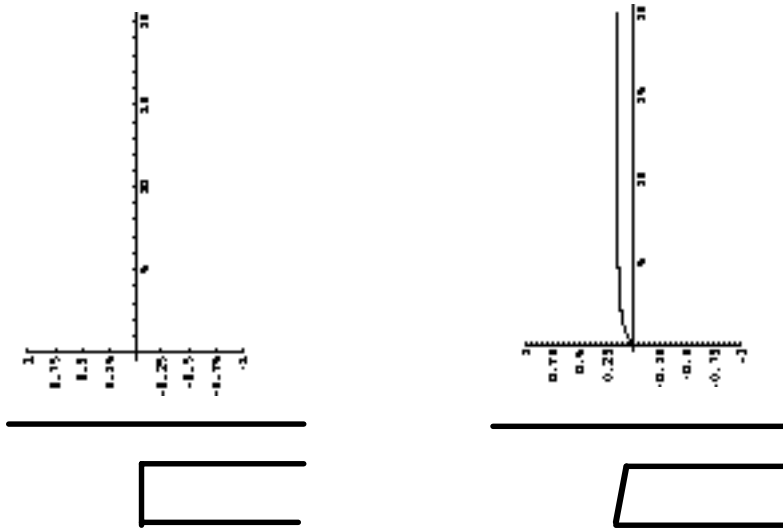


Figure 3. Vertical and almost vertical faults and multiscale edges at different heights.

3.2 Quantitative Inversion

We now turn to a numerical inversion for the position and amplitude of the multiscale edge. The aim is to recover four parameters (the dip, density contrast, and depths to top and bottom) for the synthetics of Figure 1 through Figure 3. The inversion is cast as an optimisation, employing a cost function consisting of a least square fit of candidate edges against the target edge.

In general, the problem could be nonlinear, with multiple local minima. We employ a variant of a Genetic Algorithm (GA) described in Boschetti et al. (1996). The GA is run with a population of 50 individuals, for 50 generations, with 0.8 and 0.1 as crossover and mutation rates, respectively. All tests are run five times. The best fitting results are shown in Table 1.

The tests have been run both on noise-free and noisy data. There were two noisy trials. The first set added 10% white noise to edge locations and values, and the second set added 20% noise. These noisy data correspond to relatively high noise levels in the measured profiles. Even so, edges remain identifiable.

The noise free cases give excellent results. Only small errors remain in the estimation of the bottom depth, clearly the hardest parameter to determine. The 10% noise case generates some errors in the estimation of the density contrast, while the geometry of

the fault is still well reconstructed. The 20% noise case also generates reasonable results, although the errors, as expected, are now larger. In particular, the dip of the fault is reconstructed within a “geologically reasonable” level of confidence, as is the depth to the top.

3.3 Visual Analysis of Solution Space

The ease with which the above inversions recovered the true parameters leads one to suspect that the cost function for this particular problem has a relatively simple minimum distribution (instead of multiple local minima of competitive amplitudes). Since the parameter space is “only” four-dimensional, we have a chance of successfully visualising the result. We proceed, first reducing the parameters from four to three by fixing the thickness of the fault, varying the other three parameters, and calculating the resulting misfit.

In Figure 4 through Figure 7, each window represents the misfit (represented in greyscale) for a different value of density contrast. Density contrast increases from 0.1 to 0.45 in steps of 0.05 from left to right, then top to bottom (i.e. in “reading order” for English). Within each window, the dip varies in the X direction (from -90° to $+90^\circ$ in 2.5° steps), and the depth to the top varies in the Y direction (from -10 to 0 units in 0.25 steps).

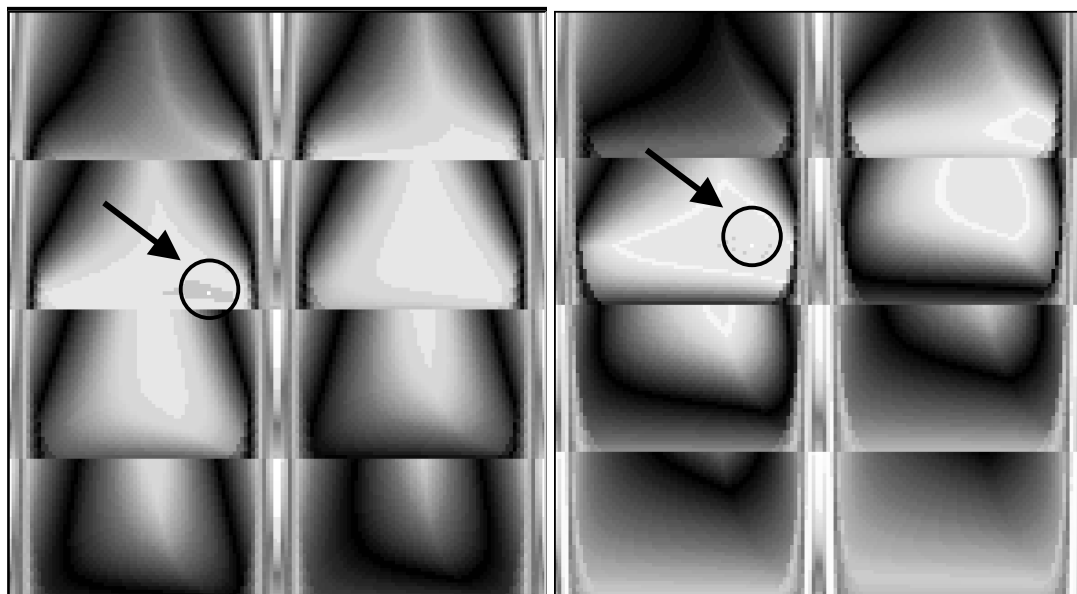


Figure 4. a) Shallow fault, dip 45 degree. b) Deep fault, dip 45 degree.

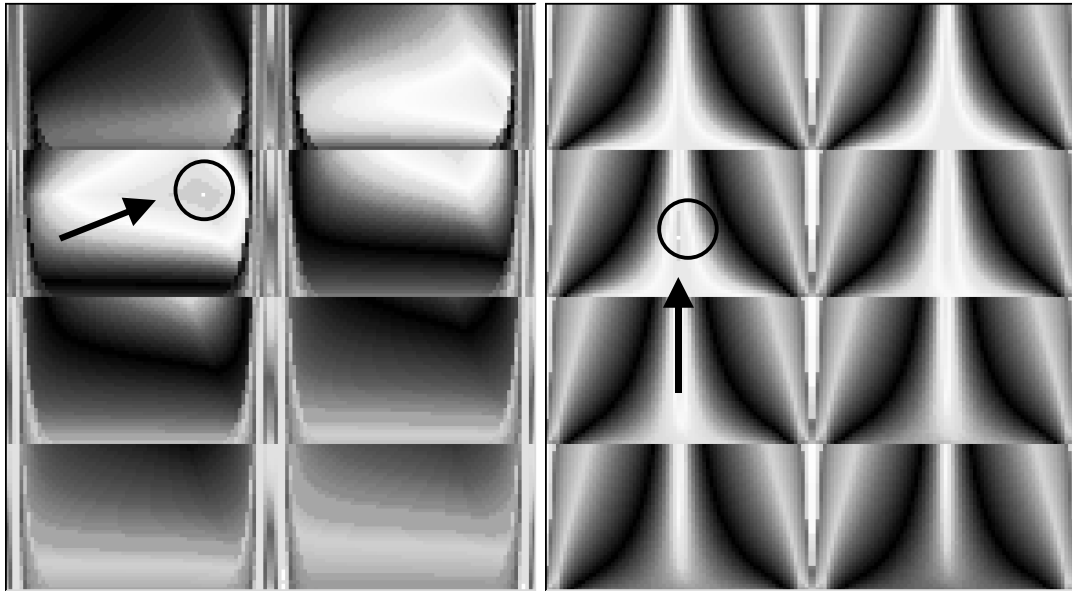


Figure 5. a) Deeper fault, dip 45 degree. b) Deep fault, dip 90 degree.

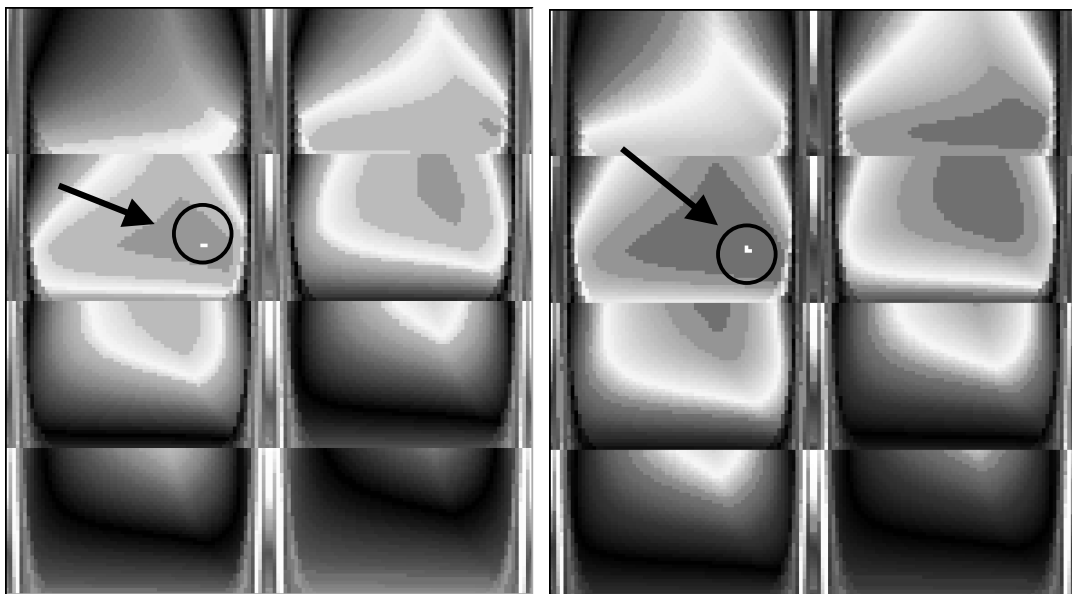


Figure 6. a) Deep fault, dip 45, +10% noise. b) Deep fault, dip 45, +20% noise.

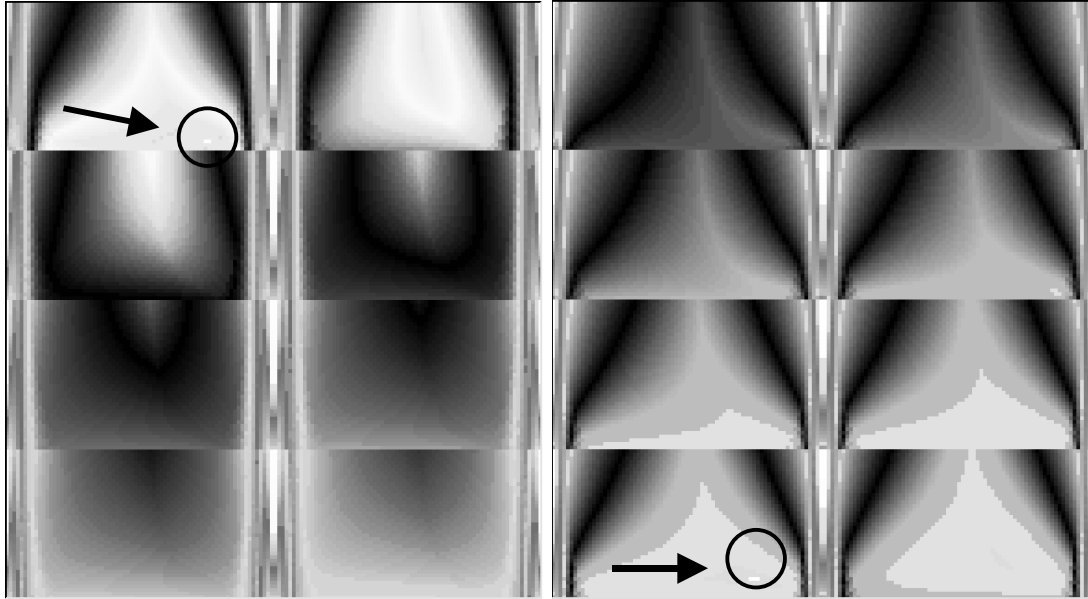


Figure 7. a) Deep fault, dip 45, thicker fault. b) Deep fault, dip 45, thinner fault.

The figures show that the inversion has a relatively simple global minimum for each case. Secondary minima do exist, near the extremes of ± 90 dips, but even a local optimiser is likely to perform well on these inversions. In view of the ambiguity domain discussed in Boschetti et al. (1999a), this is a somewhat remarkable result. Recall that the only assumptions involved were that the body was a 2-D fault-truncated horizontal layer, of constant density contrast.

The information contained in multiscale edges is sufficient to distinguish between simple source singularities. We are exploring a three part inversion strategy based upon 1) classifying a multiscale edge, 2) isolating it, using the field reconstruction properties discussed in Hornby et al. (1999), and 3) inverting it, in much the same way that we performed the fault-bounded horizontal layer inversion. Results based upon this strategy will be reported elsewhere.

4 MULTISCALE EDGE TOPOLOGY METHOD

4.1 Motivation

Consider the field due to an infinitely thin, band-like body of constant density contrast that extends to infinity in the y direction (see Figure 8a). The density contrast along the x axis is given by a step function (see Figure 8b). The constant density assumption is actually not required, but makes the presentation of the method more intuitive. Let

the body be at height $z_d \leq 0$. The gravity response at zero distance above the body is equivalent to the density distribution itself, to within a constant scale factor. Above the surface, the field is the source distribution blurred by the wavelet smoothing function, to within the same constant scale factor. Figure 9 shows such a family of upward continued gravity profiles.

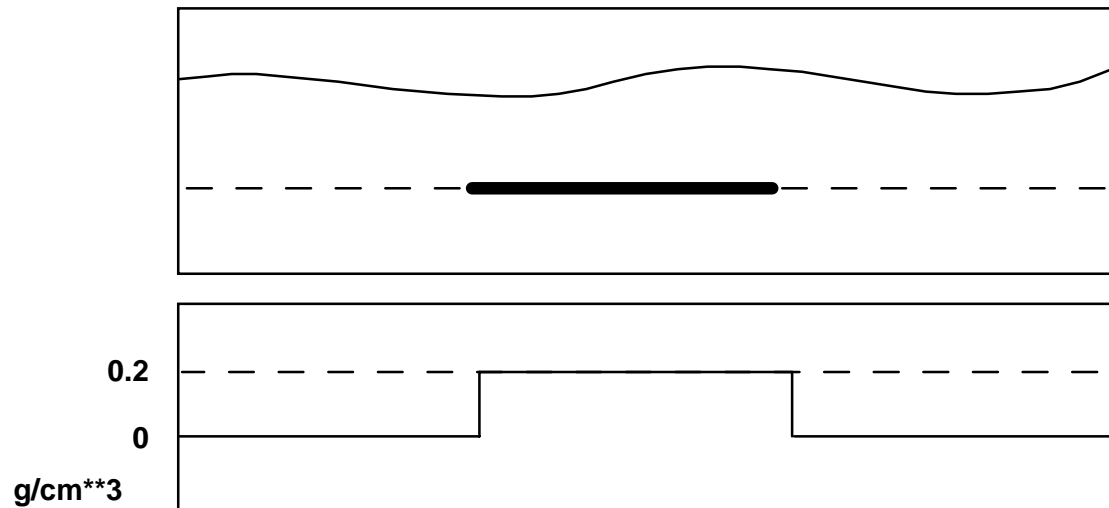


Figure 8. Infinitely thin, flat source (a) and its density distribution (b). The density contrasts at the borders of the source are characterised by a step function.

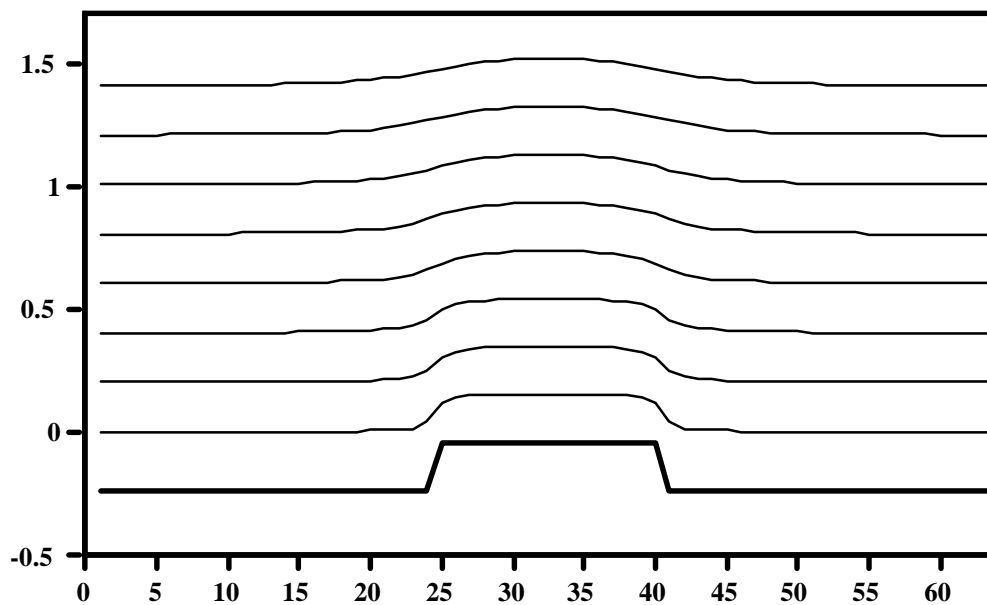


Figure 9. Density distribution (bottom line in bold) and gravity response upward continued at different levels.

In addition, the gravity profile at a certain height can also be regarded as an equivalent planar density source of further upward continued profiles (modulo the same constant scale factor as before).

Now, if we analyse the profiles in Figure 9 from top to bottom (i.e. downward continue the profiles) they get sharper. Conceptually, when we reach the source level, the profile would be the perfect step function of Figure 8b.

If we were to downward continue even farther (in the Fourier domain), the profile would become over-sharpened and begin to exhibit something akin to Gibbs phenomenon (Figure 10). The reason for this over-focusing is roughly as follows.

Define the 2-D Fourier transform by

$$\hat{f}(\vec{k}) = \int_{\mathfrak{R}^2} f(\vec{x}) \exp(-2\pi i \vec{k} \cdot \vec{x}) d\vec{x}. \quad (4.1)$$

It can be shown (e.g. Craig, 1986) that the transform of the normalised Green's function is

$$\hat{\gamma}_z(\vec{k}) = \exp(-2\pi \|\vec{k}\| |z|) \quad z > 0. \quad (4.2)$$

When we downward continue from some level z_0 to z_d say, conceptually, we have first upward continued from the source at z_d to z_0 , and then downward continued the field. The net effect is that of multiplying and then dividing the Fourier transform of the source by Equation (4.2) with $z = z_0 - z_d$. If, however, we attempt to downward continue past the source, the net effect will be a signal corresponding to the source term multiplied by Equation (4.2) for some $z < 0$. This is, of course, incorrect. In fact, the z appearing in Equation (4.2) should actually be $|z|$, and the whole expression should change sign at $z=0$ to reflect the opposite direction of the acceleration as the source is passed. (The derivation of Equation (4.2) requires a different choice of pole and contour integral in the complex k_z plane for the case $z < 0$.) The effect of such over-continuation is to introduce an oscillatory component into what is normally a smooth (elliptic) Green's function, resulting in a crossover into a regime in which oscillatory density functions begin to arise.

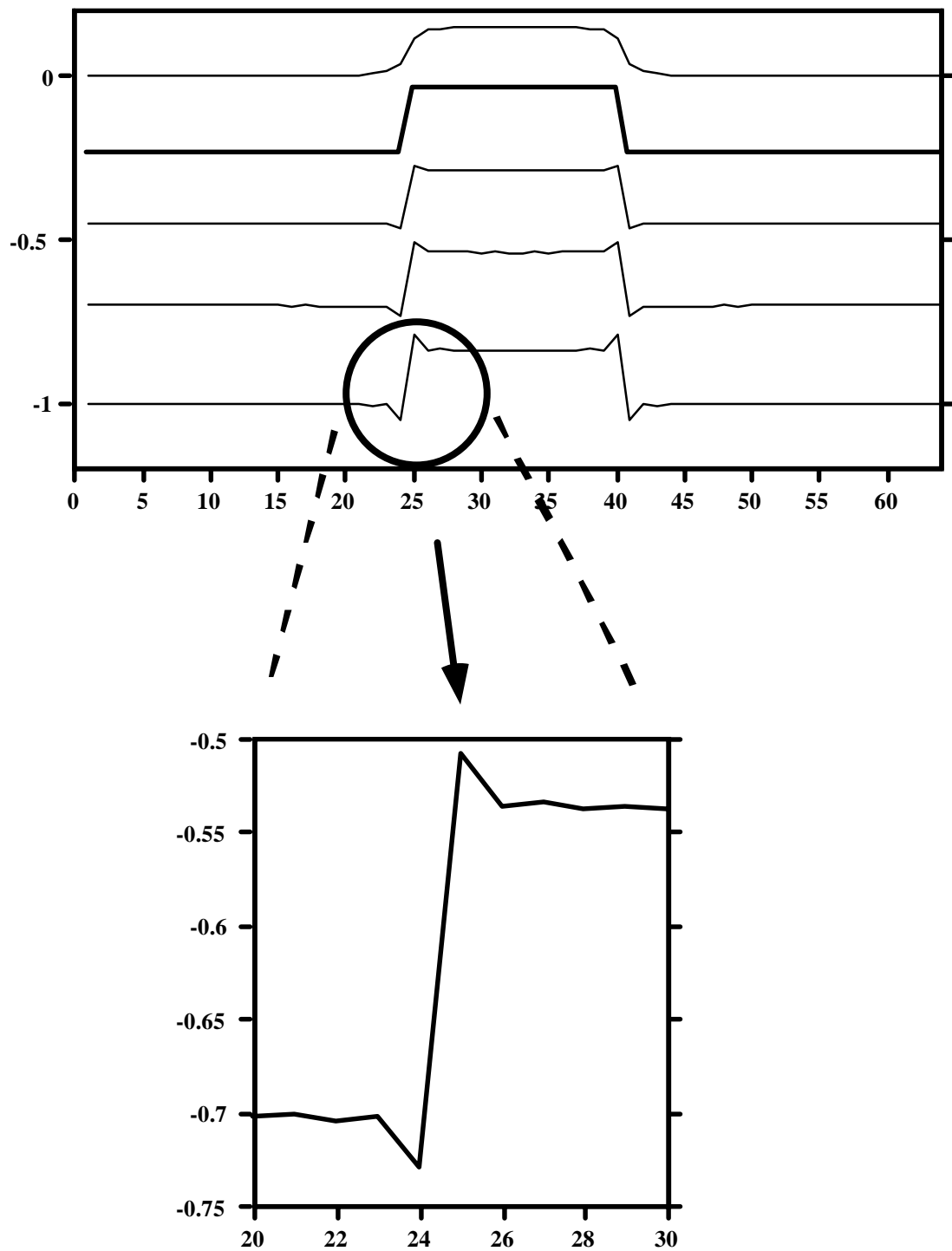


Figure 10. a) Density distribution (bold profile) and gravity response downward continued at different levels. b) Notice that, below the source level, the density contrast becomes sharper than a step function (magnification).

Physically, such over-focused density wiggles could, in principle, be real. However, applying the “rocks have edges” assumption (that sources are piecewise constant density distributions, punctuated by singularities) we reject these Gibbs-like phenomena as geologically unlikely, and interpret the behaviour as the signature for the downward continuation plane passing through the source. Hence, by developing an algorithm to identify these over-focused wiggles, we could invert for the depth to the source. Such an algorithm might be framed along the lines of: 1) downward continue the current field by a constant increment, 2) check for the presence of the over-focused wiggles, and 3) if there are wiggles, mark a source at that level and position, otherwise go to Step 1.

4.2 The ‘Trifurcation’ Point

The previous section restates a typical application of downward continuation. An anomalous field is downward continued until the anomaly comes into sharpest focus. The amount of downward continuation is then taken as the depth to the source. This section describes an algorithm for automating and localising that procedure using multiscale edges.

Multiscale edges offer a particularly straightforward method for identifying the over-focused wiggles. Because the wiggles of the type shown in Figure 10 create new local extrema in the profile, there are new local extrema in the derivative too, and the wavelet transform excels at picking these up. The multiscale edges split into three branches (“trifurcate”). Figure 11 displays the horizontal derivative of the topmost profile of Figure 10. The location of the two extrema give the position of the edges. In Figure 12 the wavelet transform of the gravity profiles at different heights is shown for the left edge. Note that at heights above or equal to the depth of the source there is only one edge. However, at levels below the source there are three edges.

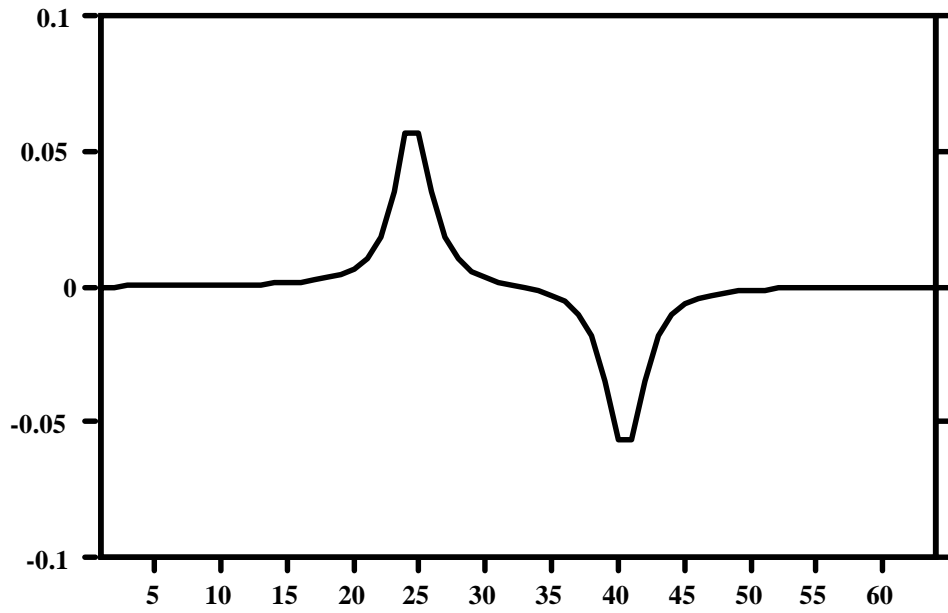


Figure 11. Horizontal derivative of the gravity profile in the above pictures. The location of the two extrema give the position of the edge.

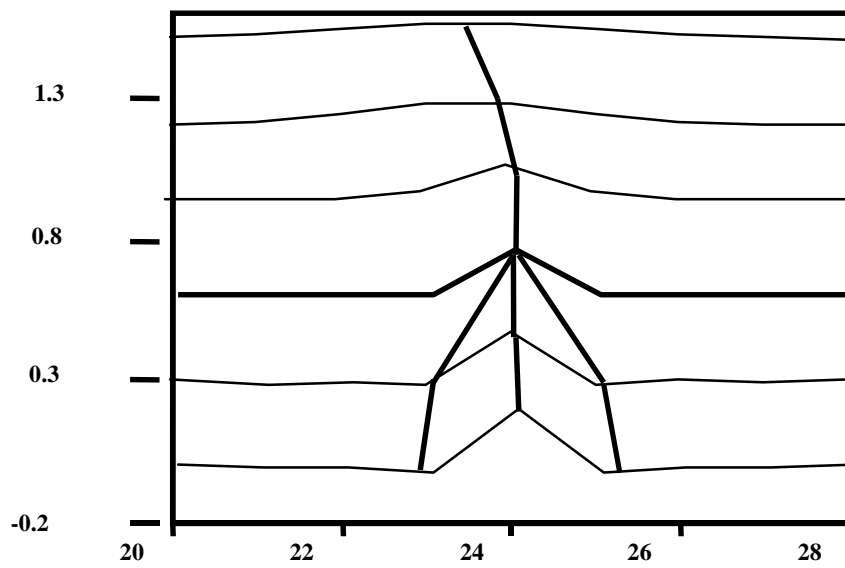


Figure 12. Wavelet transform of the gravity profiles at different heights, for the horizontal position close the left border of the source. The near-vertical dark lines show the location of the multiscale edge.

4.3 Inversion of Synthetic Examples

In the next two figures, we show inversions for some 2-D synthetic sources (represented by the white outlined bodies). All density contrasts are 0.2 g/cm^3 . The profile is modelled by 128 points equally spaced, notionally at an interval of 1 km. The inversion domain contains 32 nodes in the vertical direction, with a spacing of 100 m. The figures are vertically exaggerated. Notice the high dimensionality of the inversions (4096 degrees of freedom). They would have been computationally expensive (if feasible) had they been approached in a traditional - voxel based - manner.



Figure 13. Inversion with the trifurcation method. a) is the top pair of figures, schematically modelling a truncated dipping fault. b) is the middle pair, another truncated dipping fault. and c) is the bottom pair with a deeper truncation. The white objects in the left hand column represent the vertical sections of the sources used to generate gravity profiles. The sources have a density contrast of 0.2 g/cm^3 against the background. Each profile is sampled by 128 points equally spaced at a notional interval of 1 km. The models and the inversions contain 32 layers in the vertical direction, with a spacing of 100 m. The outline defined by the “picks” from the first trifurcation of an edge are shown in the right hand column. The figures are vertically exaggerated.

In Figure 13a, the inclined fault is picked reasonably well. At the left side, the technique has trouble with the vertical boundary. It overestimates the depth to the top. The exact location of the trifurcation point at the source depth occurs only in the perfect case of an infinitely thin source. A thicker source can be thought of as the summation of many infinitely thin layers and the resulting gravity profile is the

summation on the effect of each layer. The net result is a logarithmic singularity in the gradient of the acceleration, which is somewhat weaker than the singularity found at the edge of an equivalent layer type solution. Consequently, the onset of oscillatory behaviour is somewhat delayed.

In Figure 13b we see the same source but upside down and deeper. Similar comments apply as for the earlier case. In Figure 13c we show both a thicker body and a steeper fault, truncated at a deeper level. The algorithm does not perform as well in this more challenging case, simultaneously overestimating the depth to the top, underestimating the depth to the bottom, and having trouble resolving the dipping boundary. While the result is not as good as for Figure 13a or b, the original shape of the body is approximated by the inversion.

A last experiment is shown in Figure 14. The algorithm here is modified to join two consecutive trifurcation points in order to isolate a body. Once this is done at one level, a density contrast is assumed, the effect of such a 'slice' is calculated and removed from the original profile, and the downward continuation proceeds.

The horizontal positions of the bodies are reconstructed quite well. However, the depths are slightly overestimated because the bodies are characterised by vertical contacts. Currently this algorithm works only for such vertical contacts and research is on-going for a further generalisation. Downward continuation noise is still evident in the black and white stripes underneath the bodies. This indicates the need for a better method for estimating the 'slice' to be stripped off before downward continuing.

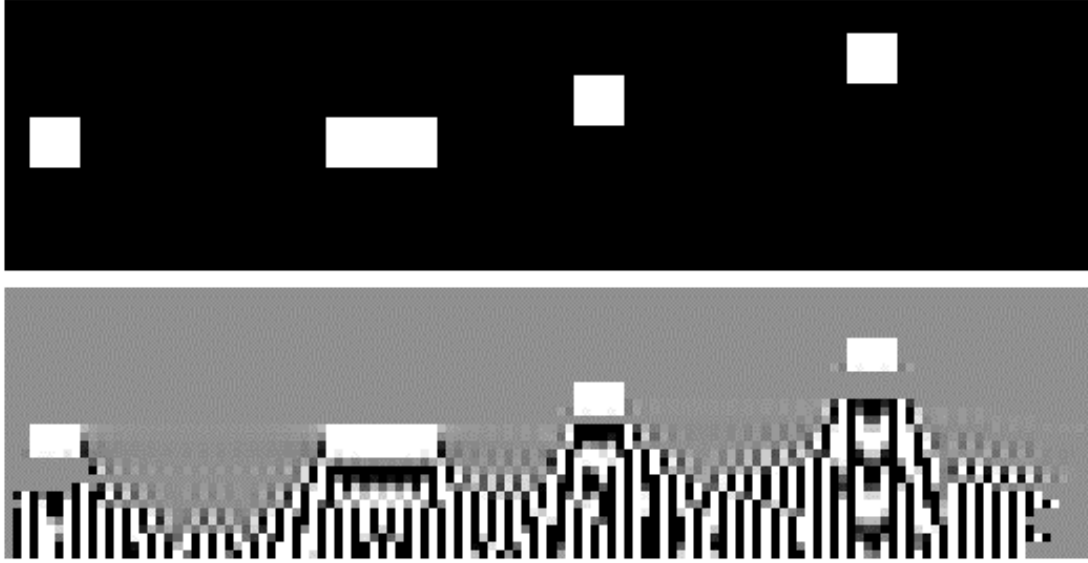


Figure 14. a) Synthetic model representing four block-like sources at different depth. b) Result from the inversion with the reconstruction of the bodies. The white stripes at the bottom are due to noise in the downward continuation.

We show the inversion experiments in Figure 14 to illustrate the potential of this approach to inversion. However, we believe that the technique shown in Figure 13 is more immediately useful.

5 INVERSE WAVELET TRANSFORM METHODS

The wavelet transform is an invertible transformation, the inverse being given by (Hornby et al., 1999)

$$f_0(\vec{x}) = 4 \int_0^\infty \frac{ds}{s} \int_{\mathbb{R}^2} (\vec{\psi}_s(\vec{u} - \vec{x}), \vec{W}[f_0](s, \vec{u}))_{\mathbb{R}^2} d\vec{u} . \quad (5.1)$$

Now, apart from normalisation by multiplicative factors of s , G , 2π and so on, the components $\psi_s^i(x, y)$ of the vector-valued wavelet are essentially the Green's functions for a mass dipole source. Thus, if we write Equation (5.1) in physical terms (i.e. put back z and the physical constants and lengths, etc.) we can interpret the equation as the field at height $z=0$ arising from a superposition of horizontally oriented gravitational dipoles. That is, *the wavelet transform itself is proportional to a possible source distribution*. We can now contemplate a variety of methods for implementing stable downward continuations and layer stripping based upon this

insight. For example, suppose we were to downward continue Equation (5.1). Then, in the integration, some of the values of s appearing in the integration would become negative, representing dipoles that are passed by the downward continuation plane. If we simply zero such wavelet coefficients, then we effectively strip these sources from the model constructed by the wavelet transform during the downward continuation process. Many variations on this theme suggest themselves, and we hope to report on this and other consequences that arise from this simple observation.

Finally, we note that the inverse transform (5.1) has a null space. This is a direct result of the linear dependence of the wavelets, regarded as a basis for functions in the (s,x) domain. It is easy to see that this null space is precisely the set of gravitational dipole source distributions that yield zero gravitational field, and is therefore, to all intents and purposes, the generator of the ambiguity domain of the original inversion problem. Thus, we have a direct characterisation of the ambiguity in the inversion problem as the null space of the inverse wavelet transform. In practice, it has proven useful to take this one step further, and consider the reproducing kernel of the wavelet transform, and its associated null space. Although the null space of the reproducing kernel turns out to be slightly larger than that of the inverse wavelet transform, the difference is trivial. However, the reproducing kernel has the added advantage of being a projection operator in the wavelet function space, and can therefore be used to construct other source distributions, obeying different *a priori* hypotheses, in a straight forward manner.

6 DISCUSSION

The inversion techniques described in Section 4 rely upon Fourier domain downward continuation, which is well known to be an unstable process. Though the process generating the over-focused wiggles described above might not be the only source of instability, it is unquestionably a principal cause.

While the Nyquist mode grows exponentially faster in Δz , it interacts with the rest of the signal's spectral content, and requires some Δz before dominating enough to generate a slope (edges) in the downward continued signal. Once initiated, a wiggle instability at any position in the data spreads throughout the entire downward continued data set with increasingly negative Δz . Clearly, this is the source of the arcuate "striping" noise in Figure 14.

The wiggle instability may also cause problems if multiple bodies are buried at different depths. Potentially, any deeper body might be masked by the noise generated by the shallower body's wiggle instability. Because of the field reconstruction properties of multiscale edges (Mallat and Zhong, 1992), one way around such problems might involve isolating anomalies by reconstructing fields due solely to the edge(s) of interest. Initial experiments in this direction have been presented in Boschetti et al. (1999b).

An additional problem related to wiggle instabilities might be found in real-world potential field surveys. Few surveys, if any, exhaustively sample the field on the grid on which final analysis takes place. Instead, the field is sampled at irregular locations (traverses, flight lines) and interpolated to the grid. While there are many techniques available to perform the interpolation (e.g. Briggs, 1974; Horowitz et al., 1996), we know of no technique that enforces the physical constraint that sources must exist underground and not above. (An exception is equivalent source gridding, which is unphysical in a different way.) The interpolation itself might lead to spurious wiggle instabilities, some of them above ground. In this context, we could in principle use wavelet based interpolation schemes to enforce the "no floating sources" constraint on the interpolation itself - instead of trying to "process them out" after doing a bad interpolation. We see then that wavelet based tools have great potential applicability.

Potential field wavelets and the multiscale edges they reveal in data yield a novel, useful, and intuitively appealing avenue for constructing inversion techniques. Starting with a simple assumption ("rocks have edges"), the ambiguity domain inherent in potential field inversions can sometimes be reduced to almost manageable proportions.

The realisation that the inverse wavelet transform implies that the wavelet transform is itself a possible source distribution, and the identification of the null space of the inverse transform as the generator of the ambiguity domain, both serve to increase our understanding of the way in which a choice of basis (Fourier, wavelet, etc.) interacts with inherent unknowability, *a priori* hypotheses, and probability densities.

7 REFERENCES

- Boschetti, F., Dentith, M. C., & List, R. D. 1996. Inversion of seismic refraction data using Genetics Algorithms. *Geophysics*, **61**, 1715-1727.
- Boschetti, F., Horowitz, F.G., and Hornby, P., 1999a. Ambiguity analysis and the constrained inversion of potential fields. Submitted to *Geophysics*.
- Boschetti, F., Hornby, P., and Horowitz, F.G., 1999b. Geophysical feature removal by multiscale edge suppression. Proceedings, 5th Int'l. Symposium Signal Process. and its Application (ISSPA99), pp935-938, Brisbane.
- Briggs, I.C., 1974. Machine contouring using minimum curvature. *Geophysics*, **39**, 39-48.
- Craig, M., 1986. The Fourier transform of $1/r$. (Short note) *Geophysics*, **51**, 417-418.
- Daubechies, I., 1992. *Ten lectures on wavelets*. SIAM, Philadelphia.
- Frieden, B.R., 1999. Physics from Fisher information: a unification. Cambridge Univ. Press, Cambridge.
- Hornby, P., Boschetti, F., and Horowitz, F.G., 1999. Analysis of potential field data in the wavelet domain", *Geophys. J. Intl.*, **137**, 175-196.
- Horowitz, F.G., Hornby, P., Bone, D., and Craig, M., 1996. Fast multidimensional interpolations. In *26th proceedings of the applications of computers and operations research in the mineral industry (APCOM 26)*, R.V. Ramani (ed.), SME, Littleton Colorado.
- Kaiser, G., 1994. *A friendly guide to wavelets*, Birkhauser, Boston, Basel, Berlin.
- Mallat, S., and Zhong, S., 1992. Characterisation of signals from multiscale edges, *IEEE Transactions on Pattern Analysis and Machine Intelligence*, **14**, 710-32.
- Moreau, F., Gibert, D., Holschneider, M., and Saracco, G., 1997. Wavelet analysis of potential fields. *Inverse Probl.*, **13**, 165-178.
- Strang, G., and Nguyen, T., 1996. *Wavelets and filter banks*. Wellesley-Cambridge, Wellesley Massachusetts.

Strykowski, G., 1996, "Dealing with the non-uniqueness of the solution to the inverse geophysical problem", , Methodology and Application in Geophysics, Astronomy, Geodesy and Physics, Proceedings to the interdisciplinary inversion workshop 4", Lyngby, 1996, Christian Hansen edition.

Sweldens, W., 1997. The lifting scheme: A construction of second generation wavelets. *SIAM J. Math. Anal.*, 29, 511-546.

8 TABLE

Type	% Noise	Density	Dip	Depth to Top	Depth to Bottom
Synthetic	--	0.2	45	-1.0	-2.0
GA Inversion	0	0.2	45	-1.1	-2.1
	10	0.16	40	-0.7	-1.9
	20	0.11	40	-0.3	-2.1
Synthetic	--	0.22	-27	-7.0	-8.0
GA Inversion	0	0.20	-25	-6.9	-9.1
	10	0.21	-25	-6.2	-7.2
	20	0.34	-25	-6.4	-7.0
Synthetic	--	0.2	90	-1.0	-4.0
GA Inversion	0	0.2	90	-1.2	-3.7
	10	0.23	90	-1.0	-3.6
	20	0.23	90	-1.0	-3.6
Synthetic	--	0.11	80	-8.0	-9.0
GA Inversion	0	0.11	80	-8.0	-9.0
	10	0.35	80	-7.6	-7.9
	20	0.35	80	-7.5	-7.8

Table 1: Results from Genetic Algorithm inversions for source parameters from multiscale edges.